Geophysical Research Letters

RESEARCH LETTER
10.1029/2023GL103525

Key Points:

- Analysis of rare earth element pattern curvature distinguishes between amphibole and garnet fractionation better than element ratios like Dy/Yb or Dy/Dy*
- Polybaric differentiation or plagioclase fractionation is unlikely to overprint a pre-existing garnet signature
- We find that garnet fractionation is not necessary for porphyry copper deposit formation

Correspondence to:
M. Anenburg,
michael.anenburg@anu.edu.au

Citation:
Tatnell, L., Anenburg, M., & Loucks, R. (2023). Porphyry copper deposit formation: Identifying garnet and amphibole fractionation with REE pattern curvature modeling. *Geophysical Research Letters*, *50*, e2023GL103525. https://doi.org/10.1029/2023GL103525

Received 3 MAR 2023
Accepted 5 JUL 2023

Porphyry Copper Deposit Formation: Identifying Garnet and Amphibole Fractionation With REE Pattern Curvature Modeling

Lucas Tatnell[1,2], Michael Anenburg[1], and Robert Loucks[2]

[1]Research School of Earth Sciences, Australian National University, Canberra, ACT, Australia, [2]Centre for Exploration Targeting, School of Earth Sciences, University of Western Australia, Crawley, WA, Australia

Abstract Porphyry copper ore-forming intrusions are distinguished from barren arc magmas by high oxidation state and "adakitic" high Sr/Y and La/Yb. Controversy over petrogenesis of adakites has centered on ambiguities in interpretation of their steep rare earth element (REE) patterns, and on whether garnet participates in their petrogenesis. Lambda (λ) coefficients deconvolute subtle differences in REE pattern curvature, providing a more quantitative method to explore mineral fractionation processes. Here, we use trace element and numerical λ coefficient modeling to assess the relative influence of amphibole, garnet, and plagioclase in the petrogenesis of porphyry ore-forming intrusions. We find that garnet-fractionation trends are not evident in REE patterns of many adakitic porphyry-forming intrusions. Instead, porphyry-forming intrusions in the western Pacific and Eocene porphyry-forming intrusions in northern Chile have REE patterns consistent with a garnet-free, amphibole-dominated cumulate. Traditional element ratios such at Dy/Dy*, La_N/Yb_N, and Dy_N/Yb_N are poor discriminants for garnet or amphibole fractionation.

Plain Language Summary Copper is a crucial metal for electrification and emission-free energy generation. Copper is primarily sourced from active and extinct volcanic mountain chains. The minerals forming in the root zones of these volcanoes are crucial for ore formation processes, but identification of the exact minerals involved in these processes is still debated. We use a novel method of detecting small variations in the chemical signature of the rare earth elements, combined with numerical modeling of mineral crystallization to distinguish the participation of two minerals, garnet and amphibole. We show that amphibole is ubiquitous whereas garnet only occurs in some deposits. Therefore, garnet fractionation is not necessary for copper deposit formation as has been previously suggested.

1. Introduction

Empirical evidence for high oxidation state of porphyry-copper-deposit (PCD) generative arc magmas has been noted and discussed for decades (Burnham & Ohmoto, 1980; Hutchinson & Dilles, 2019; Park et al., 2021). These magmas typically record oxygen fugacity (fO_2) values equal or greater than the Ni–NiO fO_2 buffer (Sun et al., 2015). The importance of high oxidation state to copper metallogenic fertility is the 10- to 20-fold increase in a silicate melt sulfur-carrying capacity as it rises into the predominance range of sulfate (Jugo et al., 2005; Park et al., 2021; Richards, 2015; Xu et al., 2022).

The cause of relatively high oxidation states in arc magmas and especially PCD-forming arc magmas relative to most other igneous suites is a topic of lively historic and continuing debate, as recently reviewed by Humphreys et al. (2015), Cottrell et al. (2021), and Métrich (2021). Recently, Tang et al. (2020) and Lee and Tang (2020) proposed that precipitation of cumulus garnet rich in the almandine component ("arclogites") is crucial for magma oxidation. As heavy rare earth elements (REE) partition strongly into garnet relative to Sr and the lighter REE, garnet fractionation was suggested to cause relatively high Sr/Y, and La/Yb in PCD-forming magmas, a chemical signature commonly referred to as "adakitic." Additionally, Tang et al. (2019) suggested that Fe^{2+} partitions into garnet preferentially to Fe^{3+}, potentially leading to the high fO_2 recorded in these rocks, a claim disputed by Holycross and Cottrell (2023). Recently, the link between garnet phenocrysts and PCD-forming dacitic intrusions in Colombia were reported by Bissig et al. (2017). Nonetheless, indication that garnet cannot be a prerequisite to all PCD-formation is given by its reduced stability in shallow crustal depths, where amphibole is the principal fractionating mineral controlling REE patterns (Chiaradia, 2015; Park et al., 2021). Garnet-free cumulates are not

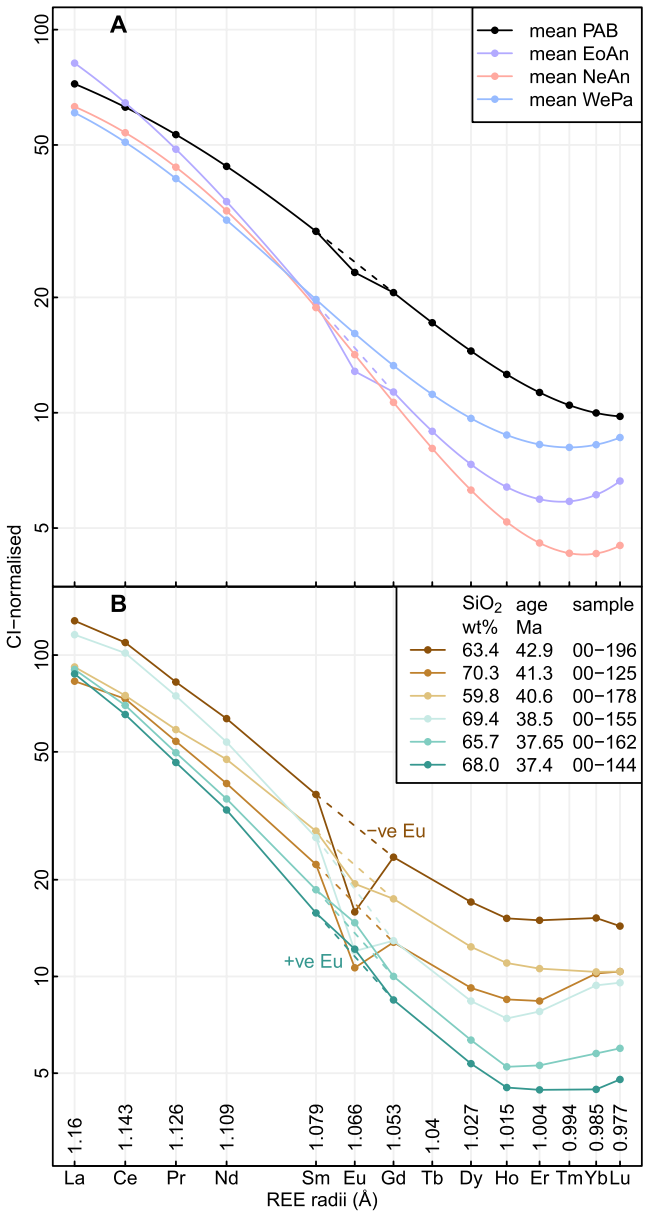

Figure 1. (a) REE patterns constructed from averaging several analyses of least-altered samples of primitive arc basalt (PAB) and PCD-forming intrusions from three different provinces: Eocene Andes (EoAn), Neogene Andes (NeAn) and Western Pacific (WePa). PCD REE patterns exhibit a HREE spoon profile, which is not necessarily diagnostic for the fractionation of amphibole or garnet, or their presence at source. (b) REE patterns in successive pre-mineralization and mineralizing intrusions in the El Abra igneous complex (Chile) reported by Ballard (2001). REE patterns rotate clockwise with younger age and fluctuating SiO_2. Eu/Eu* is strongly negative in the oldest intrusions, progressing to weakly positive in the youngest intrusions. Values are normalized using CI-chondrite values in O'Neill (2016). REE radii are from Shannon (1976). See Supporting Information S1 (https://doi.org/10.6084/m9.figshare.21431712) for a tabulation of plotted analyses and literature sources.

restricted to PCD-forming magmas and have been observed or inferred in arc magmas (Arculus & Smith, 1979; Greene et al., 2006; Tassara & Ague, 2022; Zhou et al., 2020).

Interpretation of whole-rock REE patterns that result from fractionation of garnet or amphibole is often inconclusive. For example, mean REE patterns of three PCD provinces (EoAn: Eocene Andes, NeAn: Neogene Andes, and WePa: Western Pacific) qualitatively exhibit a similar shape with LREE enrichment and a typical characteristic "spoon" profile (Figure 1a). Quantitative ratios such as La_N/Yb_N, Dy_N/Yb_N, Dy/Dy* and other REE ratios that are often used to infer amphibole or garnet fractionation (e.g., Barber et al., 2021; Davidson et al., 2007; Davidson et al., 2013; Tang et al., 2020) are not independent of the ratios present in the melting source (Anenburg, 2020). Some of this chemical signature might be inherited, complicating uncertainties regarding fractionating minerals. Additional complexities might arise from fractionating plagioclase owing to substantial differences in its REE partition coefficients and ability to impart a Eu anomaly. These confounding issues might obscure true garnet and amphibole fractionation signatures. Thus, potential benefit might be found in a method to distinguish amphibole from garnet fractionation, which we develop here using the lambda method, first introduced by O'Neill (2016).

1.1. Rare Earth Element Patterns

Lambda coefficients quantify polynomial characterization of CI-normalized REE pattern shapes, allowing deconvolution of fine-scale curvature (Anenburg, 2020; Anenburg & Williams, 2022; O'Neill, 2016). These coefficients can be combined with traditional petrogenetic modeling based on mineral/melt partition coefficients to derive "process vectors": arrows in λ-space plots that predict changes in REE pattern shape during igneous petrological processes (Ψ vectors of O'Neill, 2016). This is useful as it employs a full set of REE partition coefficients, permitting accurate quantification of small curvature differences resulting from fractionation of different minerals. Europium and Ce anomalies do not significantly affect lambda coefficients. The high resolving power of lambda coefficients is particularly useful for determining magmatic process at PCD sources because the ubiquitous high La/Yb ratio in PCDs, often explained by garnet fractionation, is a non-unique solution, and fractionation of other minerals (notably amphibole) can lead to similar chemical signatures (Barber et al., 2021; Hao et al., 2019; Lang & Titley, 1998; Nandedkar et al., 2016; Park et al., 2021; Stern et al., 2011). The lambda method shows changes in curvature during petrogenetic processes, independently of starting composition (O'Neill, 2016). Barber et al. (2021) and Leong et al. (2023) successfully used lambda (λ) coefficients to infer amphibole or garnet bearing cumulates in PCD-forming intrusions.

2. REE Pattern Modeling

2.1. Model Design and Rationale

Here, we combine the λ-coefficient method with petrogenetic modeling (O'Neill, 2016) of magma bodies differentiating at 7 kbar and at 10 kbar. We use published liquid line of descent (LLD) and trace element partitioning experiments to model three igneous processes: a single-cycle LLD, cyclic recharge fractionation (R–F), and polybaric differentiation (PBD), and compare these models with compiled data for WePa, EoAn and NeAn PCD-forming intrusions (this compilation is available in the Supporting Information S1, https://doi.org/10.6084/m9.figshare.21431712). These

localities are in arc segments above subducting oceanic lithosphere that are geodynamically well characterized and host relatively young (<40 Ma) PCDs.

PCD-forming intrusions commonly record evidence of multiple cycles of replenishment and crystallization prior to ore-formation (Ballard, 2001; Rohrlach & Loucks, 2005). As a basis for the modeling strategy, we use observations from the late Eocene El Abra Cu–Mo PCD in northern Chile. This deposit is particularly informative because its pre-ore to ore-forming intrusions faithfully record these multiple cycles (Correa et al., 2016; Rabbia et al., 2017). The rocks exhibit the temporal evolution of the El Abra underlying magma chamber with replenishments of a mafic, probably close to primitive, arc melt (Figure 1b). The replenishment and subsequent fractionation results in a ramp up of H_2O, the light REE, and other incompatible elements (Lee et al., 2014; Rohrlach & Loucks, 2005). Increasing H_2O concentration with successive replenishments is supported by the decreasing Eu/Eu* with age at El Abra (Figure 1b), interpreted to be a result of cumulus plagioclase suppression in increasingly hydrous melt crystallizing at lower-crustal pressures (Alonso-Perez et al., 2009; Loucks, 2021). Note that the lack of cumulus plagioclase segregation does not preclude late plagioclase crystallization after garnet or amphibole in response to cooling, decompression, and fluid exsolution during magma ascent (Dessimoz et al., 2011). Similar cumulus plagioclase suppression can be seen elsewhere, for example, in Tampakan, Philippines (Rohrlach & Loucks, 2005), and El Teniente, Chile (Stern et al., 2011). Early pre-ore intrusions at these deposits do, however, have initially negative Eu/Eu* indicating plagioclase fractionation at an early stage. It is difficult to estimate when segregation of cumulus plagioclase ceased. As such, four replenish–fractionation (R–F) models are provided: two at 7 and 10 kbar with a plagioclase-free cumulate wherein the plagioclase component from the relevant experiments (see below) is assumed to remain dissolved in the melt, and two models at 7 and 10 kbar wherein the plagioclase component from the relevant experiments is considered as a fractionating mineral. This provides two end members between which natural arc rocks formed by R–F processes should sit (i.e., between the expected plagioclase-bearing standard LLD of arc calc-alkali basalt and plagioclase-free fractionation in very hydrous melts).

Plagioclase-free modeling includes a 7 kbar model based on hydrous fractional crystallization experiments by Nandedkar et al. (2014) and considers REE fractionation of dominantly amphibole with minor magnetite, apatite, quartz and biotite. Additionally, a 10 kbar model based on hydrous fractional crystallization experiments by Ulmer et al. (2018) considers REE fractionation of dominantly amphibole and garnet with minor ilmenite, apatite and magnetite. The plagioclase component in experimental melts by Nandedkar et al. (2014) and Ulmer et al. (2018) was assumed to remain in the melt, based on inferred plagioclase-suppression at El Abra (Figure 1b). Two additional R–F models include late-crystallizing plagioclase as described in Nandedkar et al. (2014) and Ulmer et al. (2018).

2.2. Model Development Using the Lambda Method

The models are plotted as process vectors in plots of λ_1, λ_2, and λ_3 (Figure 2). As process vectors denote changes in REE pattern shapes, they are independent of the starting position and can be translated without affecting vector direction or magnitude. Here, we choose an average primitive arc basalt (PAB) position as the process vector starting point. This composition is also used for replenishing melt composition in the R–F models. For the LLD processes, we model the REE patterns of the melt based on the full experimental fractionation sequence as given by Nandedkar et al. (2014) and Ulmer et al. (2018): from 1170°C to 700°C for the 7 kbar model, and from 1330°C to 720°C for the 10 kbar model. For the R–F models, we consider 10 steps of starting composition (PAB) recharging the resident melt to ∼900°C and fractionating to ∼700°C for the 7 kbar model and 750°C for the 10 kbar model. This temperature range was determined based on the experiments in Nandedkar et al. (2014) that reproduce the silica contents observed in the R–F cycles of El Abra (Figure 1b). Recharge amounts are about 15% and 30% for the plagioclase-free 7 and 10 kbar models, respectively, and about 45% for both plagioclase-bearing models. These recharge fractions are based on the amount crystallized in that range (i.e., assuming constant magma chamber volume). Further details, modeling parameters, and R code to reproduce all models and figures are available in the Supporting Information S1 (https://doi.org/10.6084/m9.figshare.21431712).

A possible scenario is one wherein magma differentiates at multiple pressures (PDB). First, at depth within the stability field of garnet, followed by shallower differentiation where garnet no longer fractionates. We model a plagioclase-free R–F system where the initial three cycles are modeled at 10 kbar and the remaining seven cycles are modeled at 7 kbar (Figures 2a and 2b).

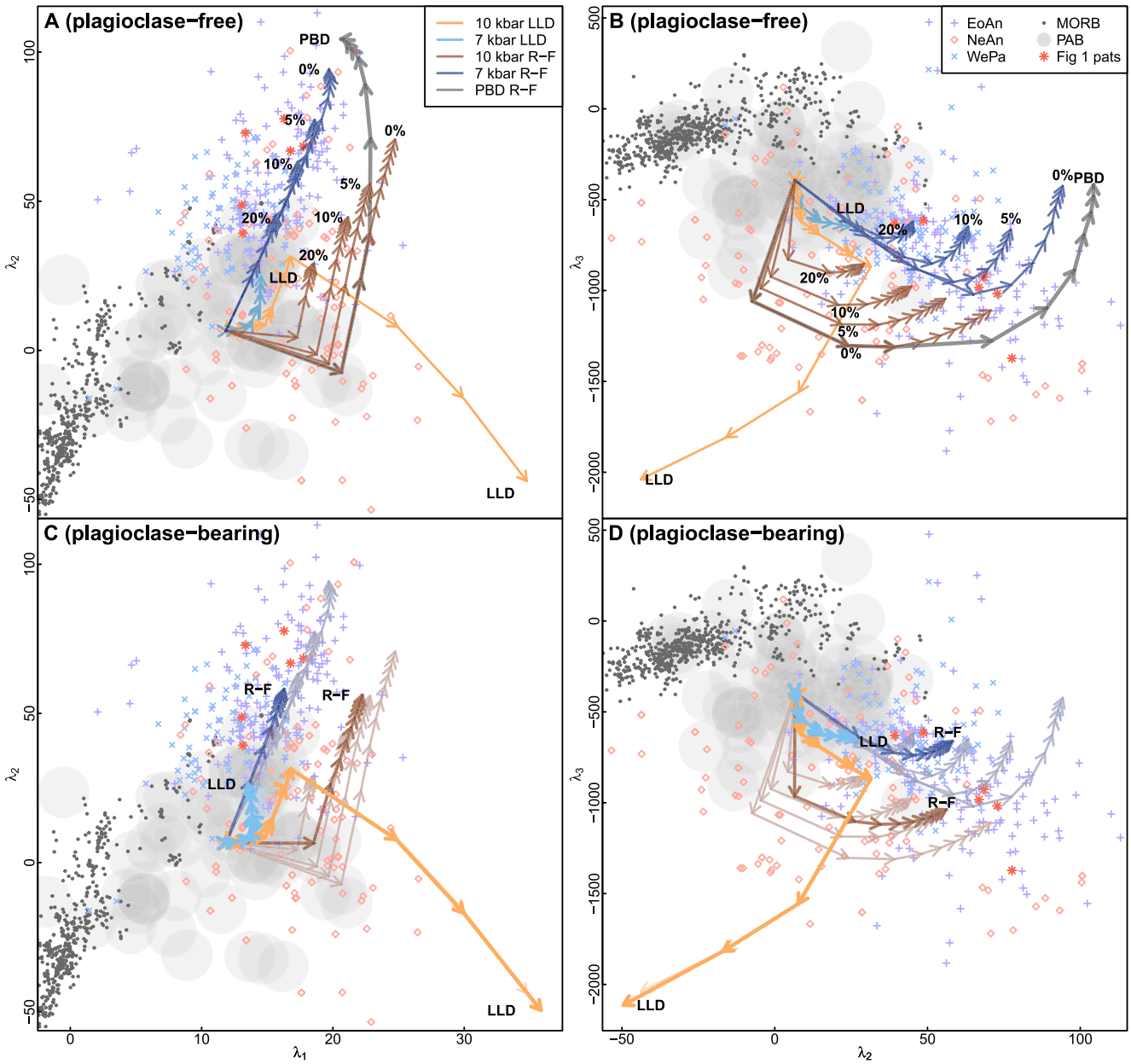

Figure 2. Lambda coefficient plots showing the REE pattern shape changes resulting from 10 cycles of replenish–fractionation (R–F) and REE pattern shape changes over a single liquid line of descent (LLD) cycle, representing REE evolution from parental calc-alkalic basalt. Each R–F arrow represents one R–F cycle between ~900 and ~700°C. Each LLD arrow represents a 30°C cooling step from 1170°C to 700°C for the 7 kbar model and 1230°C to 750°C for the 10 kbar model. Panels (a) and (c) show 7 and 10 kbar R–F and LLD models in λ_2–λ_1. B and D show 7 and 10 kbar R–F and LLD models in λ_2–λ_3. λ_1 measures linear slope, λ_2 measures quadratic curvature, and λ_3 measures cubic curvature. For (a) and (b), all models have a plagioclase-free residue. Models have variable fractions of material erupted in each cycle (expressed as percentages). For C and D, models have a plagioclase-bearing residue, and are overlayed on the plagioclase-free models for comparison (expressed as pale vectors). For all panels, Eocene Andes (EoAn), Neogene Andes (NeAn) and Western Pacific (WePa) PCD compositions are plotted, primitive arc basaltic (PAB) compositions are plotted as an approximate starting or replenishing composition, and MORB compositions are plotted as a reference frame (following O'Neill, 2016). REE patterns from Figure 1b are plotted as red stars. Interested readers can experiment with the interactive apps at https://lambdar.rses.anu.edu.au/ to gain an intuitive grasp of the lambda method and how these coefficients correspond to REE patterns (Anenburg, 2020; Anenburg & Williams, 2022; O'Neill, 2016).

3. Results and Discussion

3.1. Plagioclase-Free Differentiation

Neogene PCD-forming magmas in the Colombian and Chilean Andes (NeAn) have wide variability of REE patterns (Figure 2), starting from an overlap with PAB, to higher λ_1 (greater LREE/HREE), greater λ_2 range

(increasing quadratic curvature of REE in both directions), and more negative λ_3 (increase of cubic curvature, or spoon profile shape). These values are mostly consistent with the wide range of patterns accessible in the 10 kbar models. Importantly, some low λ_2 values in the NeAn data set can be easily reached by 10 kbar fractionation from typical PAB starting conditions but can only be reached by 7 kbar fractionation under improbable PAB starting compositions. The modeling is not conclusive for NeAn rocks with high λ_2, and these patterns can be generated by both models (i.e., with garnet at 10 kbar and without at 7 kbar). The agreement with NeAn data and 10 kbar modeling indicates that garnet-bearing pyroxenite cumulates (arclogites) are likely to exist underneath most of these deposits.

Most Eocene PCD-forming magmas in the Andes (EoAn) and Neogene PCD-forming magmas from the Western Pacific (WePa) agree with both the single-cycle LLD and R–F models at 7 kbar, which precludes garnet fractionation. Some data are offset from the process vectors but shifting the vector origin to lower λ_1 within the PAB field (i.e., source being less LREE-enriched and closer to MORB patterns) would resolve the discrepancy. These rocks are very unlikely to form via 10 kbar differentiation, as garnet fractionation pushes melt composition to lower λ_2, the opposite of the EoAn and WePa trend. The only way for these rocks to form by garnet fractionation is shifting the starting point outside the PAB field, into a non-existent extension of the enriched MORB trend. Therefore, we suggest that garnet-bearing cumulates as residues from PCD-forming magmas in EoAn and WePa are unlikely.

WePa magmas have REE patterns generally more like PABs than their EoAn analogs. The proximity of WePa data to the PAB starting composition could be explained by a higher eruption fraction than EoAn PCDs, or by plagioclase in their cumulates (Figure 2). Additionally, compiled WePa data only reaches SiO_2 contents of ~70 wt%, compared with ~75 wt% in the Andes. While this could be a result of sampling bias, it is possibly a result of less evolved PCD-forming magmas in WePa compared with Andean PCD-forming magmas. WePa data proximity to PAB starting composition could also be explained by differences in primary magma or less time to evolve after orogenic release of entrapped magma due to relatively thin island-arc crust.

3.2. Effect of Plagioclase

Figures 2c and 2d show the effect of including cumulus plagioclase from the 7 kbar Nandedkar et al. (2014) and 10 kbar Ulmer et al. (2018) experiments. Compared to the plagioclase-free modeling (Figures 2a and 2b), its inclusion mostly leads to reduction in R–F process vector magnitudes. There is very little change in vector direction and the effect of plagioclase on R–F vectors is not dissimilar to increasing erupted material fraction. HREE are incompatible in plagioclase (Bédard, 2006b) so its inclusion in modeling leads to a reduction of the bulk partition coefficient for the HREE. Additionally, LREE partition coefficients for plagioclase are greater than HREE, ($\lambda_1 > 0$) and they curve downward (i.e., a convex $\lambda_2 > 0$). This is opposite to partition coefficients for garnet and amphibole, in which the HREE are more compatible ($\lambda_1 < 0$) and consist of a concave upwards curve ($\lambda_2 < 0$) (Nandedkar et al., 2016). Therefore, inclusion of plagioclase partly negates the dominant trends imposed by garnet and amphibole but cannot cancel them or change their direction. Plagioclase fractionation could be a reason for more modest spread in the WePa PCD analyses compared to the EoAn rocks.

3.3. Polybaric Differentiation

Figures 2a and 2b shows the resulting vectors from the PBD model, where they follow the 10 kbar R–F model (as expected) until the third cycle where they begin to curve toward the 7 kbar model. After 10 cycles the model approaches the same final location as the 7 kbar model. The magnitude-reducing effects of plagioclase and eruption fractions could cause such a polybaric system to be unresolvable from garnet-free systems. However, this requires a high number of R–F cycles (10 in this case). Whether this number can be reached in a single magmatic system is currently unknown. For instance, Rohrlach and Loucks (2005) record a total of only three R–F cycles in zircons from Tampakan. Additionally, pre-ore to ore-forming intrusions are expected to progress along the R–F lines, and no data from EoAn or WePa follows the PBD vectors. We therefore consider early garnet fractionation followed by differentiation at a pressure sufficiently low to destabilize garnet unlikely in WePa and EoAn PCDs.

3.4. Garnet and Amphibole Fractionation Through Time

Our models show trends in lambda space that melt in a periodically replenished chamber should follow with successive R–F cycles. Older intrusions that have experienced less R–F cycles should thus be more similar to the

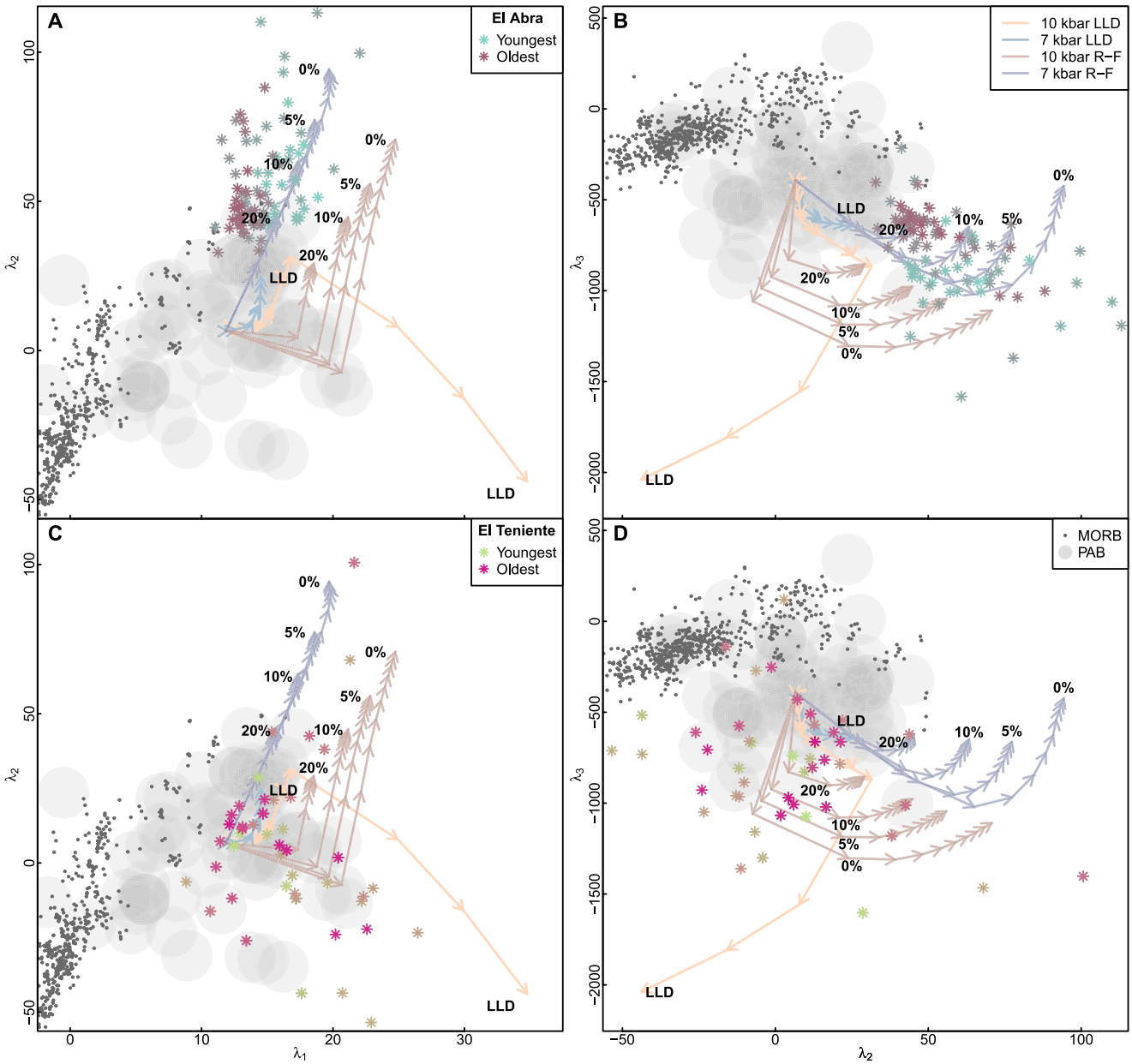

Figure 3. Plagioclase-free models replicated from Figure 2 overlayed on compiled pre-ore to ore-forming data from intrusions in the Eocene El Abra igneous complex (a and b) and the Neogene El Teniente igneous complex (c and d). Data are colored grading from the youngest age to the oldest age (El Abra: 37.4–42.9 Ma, El Teniente: 2.3–8.2 Ma).

initial composition than the younger intrusions. Figure 3 shows data from pre-ore to ore-forming intrusions at the Eocene El Abra and the Neogene El Teniente with colors graduating from the oldest to youngest intrusions related to those deposits. Additionally, El Abra REE patterns from Figure 1b are plotted in Figure 2 as red stars. Data from El Abra (Figures 3a and 3b) are entirely consistent with the garnet-free 7 kbar differentiation model, with older ages clustering toward PAB and younger ages further along the modeled trend. The trend at El Abra is slightly off the modeled trend, so the starting composition is likely higher λ_2 and lower λ_3 compared to mean PAB, around the most PAB-like point from El Abra. The high spread in the El Abra points indicates that eruption fractions were minor and little plagioclase fractionated (as these would limit the spread, Figures 2c and 2d), consistent with the gradual increase in Eu/Eu* (Figure 1b). Data from El Teniente is significantly more scattered than that of El Abra. Older ages seem to cluster toward PAB, but younger ages are scattered and do not define a clear trend. Regardless, the apparent clustering of older intrusions near PAB indicates that these intrusions did fractionate

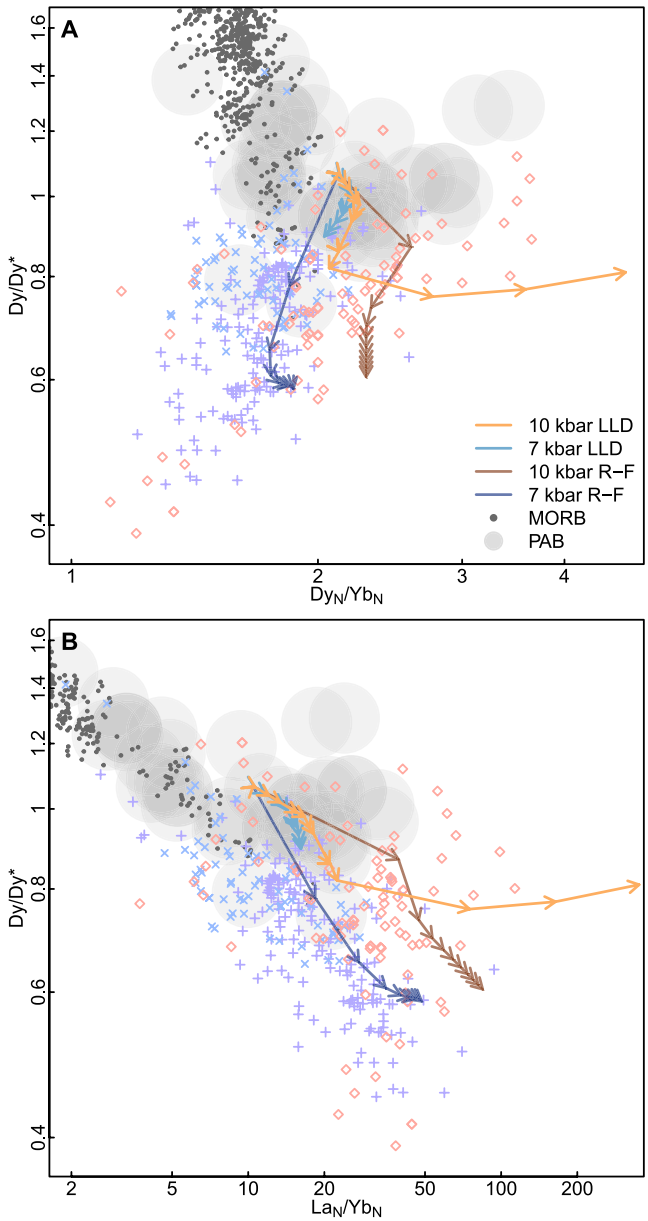

Figure 4. R–F models from Figure 2 using conventional REE element ratios. (a) Evolution of Dy_N/Yb_N and Dy/Dy* in R–F models. (b) Evolution of La_N/Yb_N and Dy/Dy* in R–F models.

at least some garnet to obtain lower λ_2 and higher λ_1, allowing distinction between garnet-bearing and garnet-free differentiation in R–F systems.

3.5. Causes for Data Scatter

We assume that measured rocks closely represent the melts from which they formed, but individual outliers and overall scatter in the data can result from occasional inclusion of cumulus phenocrysts in bulk rock analyses, or incorrect identification of rocks as PCD-forming magmas. Scatter and mismatch between natural data and models can be explained by the choice of our starting point which is merely one possible point out of many. The origin of each process vector can be translated around within the PAB field such that process vectors capture nearly the entire natural data range. Some scatter in the NeAn compilation strays from PAB toward lower λ_2 and higher λ_1. This might be attributed melting of garnet-bearing peridotite at source or assimilation of garnet-bearing eclogite or garnet amphibolite in crustal roots. However, primitive arc basalts compiled here (see Supporting Information S1, https://doi.org/10.6084/m9.figshare.21431712) do not retain evidence for melt segregation from garnet-peridotite (HREE depletion, high Sr/Y), so we find this unlikely. Alternatively, high degree melting can exhaust garnet at source, diluting these garnet signatures (e.g., Hürlimann et al., 2016), but the resolving power of the lambda method can detect subtle curvature differences (via λ_2) that indicate the former presence of garnet at source. Partial assimilation of garnet-bearing lower crustal country rock is possible but requires Sr- or Pb-isotope evidence to resolve.

3.6. Comparison With Element Ratios

Traditional element ratios are often used to distinguish various petrogenetic processes. Davidson et al. (2013) examine the three ratios La_N/Yb_N, Dy_N/Yb_N, and Dy/Dy* together with modeling, and derive some general observations regarding translating these ratios in natural rocks into the fractionating mineral identity. A commonly used ratio is Dy_N/Yb_N, with a simple rule of thumb of increasing ratios indicating garnet fractionation whereas decreasing ratios indicating amphibole fractionation. Figure 4 shows our modeling results plotted in terms of element ratios. The results are consistent with the findings of Davidson et al. (2013), but only for simple LLD models, or for the first cycle of a R–F model. For two cycles or more, we find that all three ratios vary in the same direction. Dy/Dy* decreases regardless of differentiation pressure. Additionally, Dy_N/Yb_N transitions from a decreasing to increasing trend after four to five cycles during amphibole fractionation and stops changing after three to four cycles of garnet fractionation (Figure 4b). Although the 10 and 7 kbar trends roughly follow the NeAn and WePa–EoAn data, their trends are parallel and closer than the R–F trends observed in lambda space (Figure 2). Furthermore, the data shows greater overlap and confusing parallel trends in element space (Figure 4), whereas there is much better separation in lambda-space (Figure 2). Given that a simple single cycle process is highly unlikely in long-lived magma chambers ("immortal" magmas, Loucks, 2021; e.g., Maydagán et al., 2014; Vry et al., 2010), we find that the use of lambda coefficients to track magmatic differentiation is superior to element ratios.

4. Conclusions

Our modeling indicates that garnet did not contribute to the formation of the EoAn and WePa PCDs, and garnet-bearing cumulates are unlikely to exist in their roots. Instead, we find that the principal mineral controlling REE pattern evolution in these rocks is amphibole. On the other hand, garnet most likely partici-

pated in the magmatic differentiation process that led to the formation of the NeAn rocks. Since all provinces contain PCDs, we conclude that garnet fractionation is not a prerequisite for PCD formation, consistent with the results of Holycross and Cottrell (2023) and Barber et al. (2021). Given that oxidized conditions are generally accepted as required for economic Cu mineralization, garnet fractionation is not an important oxidative process.

We show that inferring REE pattern trends in arc rock suites is better facilitated using lambda shape coefficients. Although element ratios are useful for simple single-cycle magmatic differentiation, they are non-unique and not suitable for realistic scenarios involving several cycles of magmatic recharge and fractionation.

Data Availability Statement

Data compilation of PCD geochemistry, modeling details, and code written in the R language that produces the modeling and the figures in this paper are available at the figshare data repository: https://doi.org/10.6084/m9.figshare.21431712.

Acknowledgments
This study was supported by Australian Research Council Linkage project LP190100785. We thank Nick Barber, Othmar Müntener, Osvaldo Rabbia, and an anonymous reviewer for their comments which allowed us to improve and focus this manuscript, and Quentin Williams for his editorial support. Open access publishing facilitated by Australian National University, as part of the Wiley - Australian National University agreement via the Council of Australian University Librarians.

References

Alonso-Perez, R., Müntener, O., & Ulmer, P. (2009). Igneous garnet and amphibole fractionation in the roots of island arcs: Experimental constraints on andesitic liquids. *Contributions to Mineralogy and Petrology*, *157*(4), 541–558. https://doi.org/10.1007/s00410-008-0351-8

Anenburg, M. (2020). Rare earth mineral diversity controlled by REE pattern shapes. *Mineralogical Magazine*, *84*(5), 629–639. https://doi.org/10.1180/mgm.2020.70

Anenburg, M., & Williams, M. J. (2022). Quantifying the tetrad effect, shape components, and Ce–Eu–Gd anomalies in rare earth element patterns. *Mathematical Geosciences*, *54*(1), 47–70. https://doi.org/10.1007/s11004-021-09959-5

Arculus, R. J., & Smith, D. J. (1979). Eclogite, pyroxenite and amphibolite inclusions in the Sullivan Buttes Latite, Chino Valley, Yavari County, Arizona. In F. R. Boyd & H. O. A. Meyer (Eds.), *The mantle sample: Inclusion in Kimberlites and other volcanics, special publication series* (Vol. 16, pp. 309–317). American Geophysical Union. https://doi.org/10.1029/SP016p0309

Ballard, J. R. (2001). *A comparative study between the geochemistry of ore-bearing and barren calc-alkaline intrusions (PhD)*. Australian National University. https://doi.org/10.25911/5d78db47e57f9

Barber, N. D., Edmonds, M., Jenner, F., Audétat, A., & Williams, H. (2021). Amphibole control on copper systematics in arcs: Insights from the analysis of global datasets. *Geochimica et Cosmochimica Acta*, *307*, 192–211. https://doi.org/10.1016/j.gca.2021.05.034

Bédard, J. H. (2006b). Trace element partitioning in plagioclase feldspar. *Geochimica et Cosmochimica Acta*, *70*(14), 3717–3742. https://doi.org/10.1016/j.gca.2006.05.003

Bissig, T., Leal-Mejía, H., Stevens, R. B., & Hart, C. J. R. (2017). High Sr/Y magma petrogenesis and the link to porphyry mineralization as revealed by garnet-bearing I-type granodiorite porphyries of the Middle Cauca Au-Cu Belt, Colombia. *Economic Geology*, *112*(3), 551–568. https://doi.org/10.2113/econgeo.112.3.551

Burnham, C. W., & Ohmoto, H. (1980). Late-stage processes of felsic magmatism. In *Society of mining geologists Japan special issue* (Vol. 8). The Society of Resource Geology. Retrieved from https://www.resource-geology.jp/special_i

Chiaradia, M. (2015). Crustal thickness control on Sr/Y signatures of recent arc magmas: An Earth scale perspective. *Scientific Reports*, *5*(1), 8115. https://doi.org/10.1038/srep08115

Correa, K. J., Rabbia, O. M., Hernández, L. B., Selby, D., & Astengo, M. (2016). The timing of magmatism and ore formation in the El Abra porphyry copper deposit, Northern Chile: Implications for long-lived multiple-event magmatic-hydrothermal porphyry systems. *Economic Geology*, *111*(1), 1–28. https://doi.org/10.2113/econgeo.111.1.1

Cottrell, E., Birner, S. K., Brounce, M., Davis, F. A., Waters, L. E., & Kelley, K. A. (2021). Oxygen fugacity across tectonic settings. In R. Moretti & D. R. Neuville (Eds.), *Magma redox geochemistry, geophysical monograph series* (Vol. 266, pp. 33–61). Wiley-American Geophysical Union. https://doi.org/10.1002/9781119473206.ch3

Davidson, J., Turner, S., Handley, H., Macpherson, C., & Dosseto, A. (2007). Amphibole "sponge" in arc crust? *Geology*, *35*(9), 787–790. https://doi.org/10.1130/g23637a.1

Davidson, J., Turner, S., & Plank, T. (2013). Dy/Dy*: Variations arising from mantle sources and petrogenetic processes. *Journal of Petrology*, *54*(3), 525–537. https://doi.org/10.1093/petrology/egs076

Dessimoz, M., Müntener, O., & Ulmer, P. (2011). A case for hornblende dominated fractionation of arc magmas: The Chelan complex (Washington Cascades). *Contributions to Mineralogy and Petrology*, *163*(4), 567–589. https://doi.org/10.1007/s00410-011-0685-5

Greene, A. R., DeBari, S. M., Kelemen, P. B., Blusztajn, J., & Clift, P. D. (2006). A detailed geochemical study of island arc crust: The Talkeetna arc section, south–central Alaska. *Journal of Petrology*, *47*(6), 1051–1093. https://doi.org/10.1093/petrology/egl002

Hao, H., Campbell, I. H., Richards, J. P., Nakamura, E., & Sakaguchi, C. (2019). Platinum-group element geochemistry of the Escondida igneous suites, northern Chile: Implications for ore formation. *Journal of Petrology*, *60*(3), 487–514. https://doi.org/10.1093/petrology/egz004

Holycross, M., & Cottrell, E. (2023). Garnet crystallization does not drive oxidation at arcs. *Science*, *380*(6644), 506–509. https://doi.org/10.1126/science.ade3418

Humphreys, M. C. S., Brooker, R. A., Fraser, D. G., Burgisser, A., Mangan, M. T., & McCammon, C. (2015). Coupled interactions between volatile activity and Fe oxidation state during arc crustal processes. *Journal of Petrology*, *56*(4), 795–814. https://doi.org/10.1093/petrology/egv017

Hürlimann, N., Müntener, O., Ulmer, P., Nandedkar, R., Chiaradia, M., & Ovtcharova, M. (2016). Primary magmas in continental arcs and their differentiated products: Petrology of a post-plutonic dyke suite in the Tertiary Adamello batholith (Alps). *Journal of Petrology*, *57*(3), 495–534. https://doi.org/10.1093/petrology/egw016

Hutchinson, M. C., & Dilles, J. H. (2019). Evidence for magmatic anhydrite in porphyry copper intrusions. *Economic Geology*, *114*(1), 143–152. https://doi.org/10.5382/econgeo.2019.4624

Jugo, P. J., Luth, R. W., & Richards, J. P. (2005). Experimental data on the speciation of sulfur as a function of oxygen fugacity in basaltic melts. *Geochimica et Cosmochimica Acta*, *69*(2), 497–503. https://doi.org/10.1016/j.gca.2004.07.011

Lang, J. R., & Titley, S. R. (1998). Isotopic and geochemical characteristics of Laramide magmatic systems in Arizona and implications for the genesis of porphyry copper deposits. *Economic Geology*, *93*(2), 138–170. https://doi.org/10.2113/gsecongeo.93.2.138

Lee, C.-T. A., Lee, T. C., & Wu, C.-T. (2014). Modeling the compositional evolution of recharging, evacuating, and fractionating (REFC) magma chambers: Implications for differentiation of arc magmas. *Geochimica et Cosmochimica Acta*, *143*, 8–22. https://doi.org/10.1016/j.gca.2013.08.009

Lee, C.-T. A., & Tang, M. (2020). How to make porphyry copper deposits. *Earth and Planetary Science Letters*, *529*, 115868. https://doi.org/10.1016/j.epsl.2019.115868

Leong, T. S. J., Mavrogenes, J. A., & Arculus, R. J. (2023). Water-sulfur-rich, oxidised adakite magmas are likely porphyry copper progenitors. *Scientific Reports*, *13*(1), 5078. https://doi.org/10.1038/s41598-023-31736-z

Loucks, R. R. (2021). Deep entrapment of buoyant magmas by orogenic tectonic stress: Its role in producing continental crust, adakites, and porphyry copper deposits. *Earth-Science Reviews*, *220*, 103744. https://doi.org/10.1016/j.earscirev.2021.103744

Maydagán, L., Franchini, M., Chiaradia, M., Dilles, J., & Rey, R. (2014). The altar porphyry Cu-(Au-Mo) deposit (Argentina): A complex magmatic-hydrothermal system with evidence of recharge processes. *Economic Geology*, *109*(3), 621–641. https://doi.org/10.2113/econgeo.109.3.621

Métrich, N. (2021). Redox state of volatiles and their relationships with iron in silicate melts. In R. Moretti & D. R. Neuville (Eds.), *Magma redox geochemistry, geophysical monograph series* (Vol. 266, pp. 215–232). Wiley-American Geophysical Union. https://doi.org/10.1002/9781119473206.ch11

Nandedkar, R. H., Hürlimann, N., Ulmer, P., & Müntener, O. (2016). Amphibole–melt trace element partitioning of fractionating calc-alkaline magmas in the lower crust: An experimental study. *Contributions to Mineralogy and Petrology*, *171*(8–9), 71. https://doi.org/10.1007/s00410-016-1278-0

Nandedkar, R. H., Ulmer, P., & Müntener, O. (2014). Fractional crystallization of primitive, hydrous arc magmas: An experimental study at 0.7 GPa. *Contributions to Mineralogy and Petrology*, *167*(6), 1015. https://doi.org/10.1007/s00410-014-1015-5

O'Neill, H. S. C. (2016). The smoothness and shapes of chondrite-normalized rare earth element patterns in basalts. *Journal of Petrology*, *57*(8), 1463–1508. https://doi.org/10.1093/petrology/egw047

Park, J.-W., Campbell, I. H., Chiaradia, M., Hao, H., & Lee, C.-T. (2021). Crustal magmatic controls on the formation of porphyry copper deposits. *Nature Reviews Earth & Environment*, *2*(8), 542–557. https://doi.org/10.1038/s43017-021-00182-8

Rabbia, O. M., Correa, K. J., Hernández, L. B., & Ulrich, T. (2017). "Normal" to adakite-like arc magmatism associated with the El Abra porphyry copper deposit, Central Andes, Northern Chile. *International Journal of Earth Sciences*, *106*(8), 2687–2711. https://doi.org/10.1007/s00531-017-1454-0

Richards, J. P. (2015). The oxidation state, and sulfur and Cu contents of arc magmas: Implications for metallogeny. *Lithos*, *233*, 27–45. https://doi.org/10.1016/j.lithos.2014.12.011

Rohrlach, B. D., & Loucks, R. R. (2005). Multi-million-year cyclic ramp-up of volatiles in a lower-crustal magma reservoir trapped below the Tampakan copper–gold deposit by Mio–Pliocene crustal compression in the southern Philippines. In T. M. Porter (Ed.), *Super porphyry copper & gold deposits—A global perspective* (Vol. 2, pp. 369–407). PCG Publishing. Retrieved from http://portergeo.com.au/publishing/superporphyry/Abstract093sp.asp

Shannon, R. D. (1976). Revised effective ionic radii and systematic studies of interatomic distances in halides and chalcogenides. *Acta Crystallographica Section A*, *32*(5), 751–767. https://doi.org/10.1107/s0567739476001551

Stern, C. R., Skewes, M. A., & Arévalo, A. (2011). Magmatic evolution of the giant El Teniente Cu–Mo deposit, central Chile. *Journal of Petrology*, *52*(7–8), 1591–1617. https://doi.org/10.1093/petrology/egq029

Sun, W., Huang, R.-F., Li, H., Hu, Y.-B., Zhang, C.-C., Sun, S.-J., et al. (2015). Porphyry deposits and oxidized magmas. *Ore Geology Reviews*, *65*, 97–131. https://doi.org/10.1016/j.oregeorev.2014.09.004

Tang, M., Lee, C. A., Ji, W. Q., Wang, R., & Costin, G. (2020). Crustal thickening and endogenic oxidation of magmatic sulfur. *Science Advances*, *6*(31), eaba6342. https://doi.org/10.1126/sciadv.aba6342

Tang, M., Lee, C.-T. A., Costin, G., & Höfer, H. E. (2019). Recycling reduced iron at the base of magmatic orogens. *Earth and Planetary Science Letters*, *528*, 115827. https://doi.org/10.1016/j.epsl.2019.115827

Tassara, S., & Ague, J. J. (2022). A role for crustal assimilation in the formation of copper-rich reservoirs at the base of continental arcs. *Economic Geology*, *117*(7), 1481–1496. https://doi.org/10.5382/econgeo.4975

Ulmer, P., Kaegi, R., & Müntener, O. (2018). Experimentally derived intermediate to silica-rich arc magmas by fractional and equilibrium crystallization at 1.0 GPa: An evaluation of phase relationships, compositions, liquid lines of descent and oxygen fugacity. *Journal of Petrology*, *59*(1), 11–58. https://doi.org/10.1093/petrology/egy017

Vry, V. H., Wilkinson, J. J., Seguel, J., & Millan, J. (2010). Multistage intrusion, brecciation, and veining at El Teniente, Chile: Evolution of a nested porphyry system. *Economic Geology*, *105*(1), 119–153. https://doi.org/10.2113/gsecongeo.105.1.119

Xu, T., Liu, X., Xiong, X., & Wang, J. (2022). Sulfur dissolution capacity of highly hydrated and fluid-saturated dacitic magmas at the lower crust and implications for porphyry deposit formation. *Geochimica et Cosmochimica Acta*, *333*, 107–123. https://doi.org/10.1016/j.gca.2022.07.004

Zhou, J.-S., Yang, Z.-S., Hou, Z.-Q., & Wang, Q. (2020). Amphibole-rich cumulate xenoliths in the Zhazhalong intrusive suite, Gangdese arc: Implications for the role of amphibole fractionation during magma evolution. *American Mineralogist*, *105*(2), 262–275. https://doi.org/10.2138/am-2020-7199

References From the Supporting Information

Bédard, J. H. (2006a). A catalytic delamination-driven model for coupled genesis of Archaean crust and sub-continental lithospheric mantle. *Geochimica et Cosmochimica Acta*, *70*(5), 1188–1214. https://doi.org/10.1016/j.gca.2005.11.008

Garrido, I., Cembrano, J., Siña, A., Stedman, P., & Yáñez, G. (2002). High magma oxidation state and bulk crustal shortening: Key factors in the genesis of Andean porphyry copper deposits, central Chile (31-34°S). *Revista Geologica de Chile*, *29*(1), 43–54. https://doi.org/10.4067/s0716-02082002000100003

Klein, M., Stosch, H. G., & Seck, H. A. (1997). Partitioning of high field-strength and rare-Earth elements between amphibole and quartz-dioritic to tonalitic melts: An experimental study. *Chemical Geology*, *138*(3–4), 257–271. https://doi.org/10.1016/s0009-2541(97)00019-3

Klein, M., Stosch, H. G., Seck, H. A., & Shimizu, N. (2000). Experimental partitioning of high field strength and rare earth elements between clinopyroxene and garnet in andesitic to tonalitic systems. *Geochimica et Cosmochimica Acta*, *64*(1), 99–115. https://doi.org/10.1016/s0016-7037(99)00178-7

Mpodozis, C., & Cornejo, P. (2012). Cenozoic tectonics and porphyry copper systems of the Chilean Andes. In J. W. Hedenquist, M. Harris, & F. Camus (Eds.), *Geology and genesis of major copper deposits and districts of the world* (Vol. 16). Society of Economic Geologists. https://doi.org/10.5382/sp.16.14

Schmidt, M. W., & Jagoutz, O. (2017). The global systematics of primitive arc melts. *Geochemistry, Geophysics, Geosystems*, *18*(8), 2817–2854. https://doi.org/10.1002/2016gc006699

Shaw, D. M. (2006). *Trace elements in magmas: A theoretical treatment*. Cambridge University Press.